THE JOURNAL OF PHYSICAL CHEMISTRY B

Article

pubs.acs.org/JPCB

Final-State Projection Method in Charge-Transfer Multiplet Calculations: An Analysis of Ti L-Edge Absorption Spectra

Thomas Kroll,*[,†,‡] Edward I. Solomon,*[,‡,§] and Frank M. F. de Groot*[,∥]

[†]Linac Coherent Light Source, SLAC National Accelerator Laboratory and [§]Stanford Synchrotron Radiation Lightsource, SLAC National Accelerator Laboratory, Stanford University, Menlo Park, California 94025, United States

[‡]Department of Chemistry, Stanford University, Stanford, California 94305, United States

[∥]Department of Inorganic Chemistry and Catalysis, Utrecht University, Universiteitsweg 99, 3584 CG Utrecht, Netherlands

Supporting Information

ABSTRACT: A projection method to determine the final-state configuration character of all peaks in a charge transfer multiplet calculation of a 2p X-ray absorption spectrum is presented using a d^0 system as an example. The projection method is used to identify the most important influences on spectral shape and to map out the configuration weights. The spectral shape of a 2p X-ray absorption or $L_{2,3}$-edge spectrum is largely determined by the ratio of the 2p core-hole interactions relative to the 2p3d atomic multiplet interaction. This leads to a nontrivial spectral assignment, which makes a detailed theoretical description of experimental spectra valuable for the analysis of bonding.

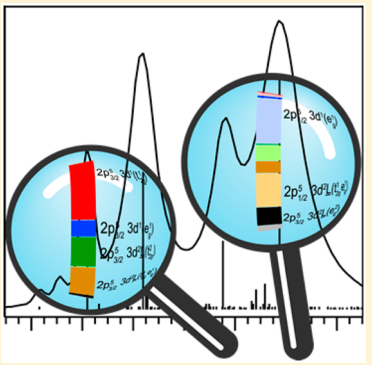

I. INTRODUCTION

The results of experiments that include the excitation of a core electron, either in an X-ray absorption (XAS) or an X-ray photoemission (XPS) experiment, exhibit a complex spectral shape that requires extensive theoretical calculations. In addition to general information such as the valence, spin, orbital occupation, and differential orbital covalency, a more detailed assignment of each final-state spectral feature is often desired. Experiments such as XAS, core XPS, and core-to-core resonant inelastic X-ray scattering (RIXS) all contain a core-hole in their final state that significantly affects the spectral shape. In other words, the spectral shape is mainly determined by the final state. Excitations of transition metal ions are further affected by atomic multiplet effects. These originate from the 3d3d as well as core-hole-3d Coulomb and exchange interactions, making a detailed understanding of the spectral shape even more challenging to acquire.

$L_{2,3}$-edge XAS spectra of transition metal ions consist of two distinct intensity regions split by the spin−orbit coupling of the 2p core-hole. It increases from 3.7 eV for Ti to 13.5 eV for Cu. Figure 1 shows the experimental result for $SrTiO_3$ (Ti(IV), $3d^0$).[1] The separation into the L_3 edge ($2p_{3/2}$) at ≈454−460 eV and the L_2 edge ($2p_{1/2}$) at ≈460−466 eV is visible. The cubic crystal field in $SrTiO_3$ splits the orbitals into t_{2g} and e_g manifolds, which is reflected by a peak splitting, visible in Figure 1, for the experimental data as well as their simulation.[2] However, the interpretation of the data is not that straightforward, given that there are more than the four main features in the spectra (see Figure 1). The reason for this

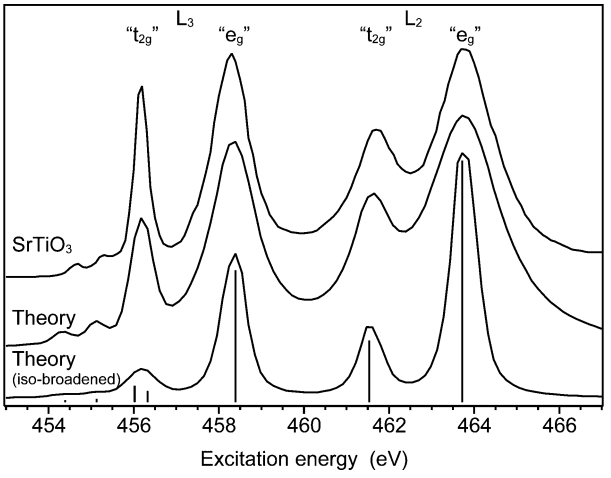

Figure 1. Experimental L-edge absorption spectrum of $SrTiO_3$ [1] (top) compared to multiplet simulations. The middle curve is simulated with varied broadening while the bottom curve uses an iso-broadening throughout the whole spectrum. The seven final-state intensity sticks apply to both theoretical curves.

Special Issue: Wolfgang Lubitz Festschrift

Received: April 30, 2015
Revised: July 14, 2015
Published: July 30, 2015

DOI: 10.1021/acs.jpcb.5b04133
J. Phys. Chem. B 2015, 119, 13852−13858

originates from the existence of the 2p core-hole in the final states, which interacts with the 3d electrons and results in additional multiplet splitting of several eV.

$L_{2,3}$-edge XAS spectra have been interpreted by various methods in the past in qualitative and quantitative ways. The branching ratio $L_3/(L_2 + L_3)$ has been used to determine spin states;[3,4] general information concerning spin and oxidation state have been determined from the qualitative comparison between spectra of known and unknown complexes;[5] the total intensity has been used as a measure of metal d-character;[6] and matrix element analysis for polarization-dependent L-edge absorption[7] as well as full multiplet calculations has been used to determine valence,[8] spin states,[9−12] ground-state symmetry and orbital occupation,[13,14] and differential orbital covalency.[6] The quantitative nature of each final-state peak, however, is usually not analyzed in detail. In addition, multiple ab initio approaches have been performed in the past.[15−23] Recently, restricted active space and restricted open-shell calculations have been used to calculate L-edge XAS spectra, including a final-state analysis.[24,25]

In this study, the focus is on the analysis of $L_{2,3}$-edge XAS spectra using multiplet calculations on Ti(IV) ($3d^0$) as an example. The final-state projection method as implemented in the TT-multiplet program[26] will be used, the wave function of each of the final states is analyzed, and the character is interpreted in terms of orbital occupation and covalency. In the Theoretical Method section, the projection method is introduced and is then used in the Results and Discussion section on Ti(IV) ($3d^0$) L-edge XAS calculations. This is done first without charge-transfer configuration interaction, i.e., before ligand covalent mixing is included, followed by a discussion of the resulting spectral changes after including ligand covalent bonding.

II. THEORETICAL METHOD

Charge-transfer multiplet calculations were performed using the atomic theory developed by Cowan[27] and the crystal field symmetry interactions described by Butler[28] in O_h symmetry, including electronic Coulomb interactions and spin−orbit coupling for each subshell.[2,10,29] The Slater−Condon−Shortley parameters F_i and G_i were reduced to 80% of their Hartree−Fock calculated values to account for the overestimation of electron−electron repulsion found in the calculations of the free ion, unless stated otherwise.[10,30,31] Covalent mixing of the metal valence is simulated using a valence bond configuration interaction (VBCI) description as implemented by Thole et al.[32] using the exact diagonalization method.[33] A two-configuration model is used by adding a ligand-to-metal charge-transfer configuration $d^{n+1}\underline{L}$ to a d^n configuration in the ground state, where $\underline{L}$ denotes a ligand hole. The corresponding charge-transfer energy Δ is defined as the difference between the center of masses of the two multiplet sets $\Delta = E(d^{n+1}\underline{L})\text{-}E(d^n)$. The effective charge-transfer energy Δ_{eff} is defined as the energy difference between the lowest energy state of both configurations.

Theoretical spectra were broadened by a Gaussian to include the experimental contribution and a Lorentzian to account for the lifetime contribution. For the simulation in Figure 1 (middle curve), a Gaussian broadening HWHM of 0.15 eV and a Lorentzian broadening HWHM between 0.1 and 1.0 eV have been used for the inclusion of solid-state effects.[9,34] For the final-state projection simulations, however, a constant broadening of 0.2 eV HWHM for both Gaussian and Lorentzian broadening was used for the sake of simplicity and visibility of spectral changes. The resulting spectrum is shown in Figure 1 (bottom curve).

The Ti(IV) $L_{2,3}$-edge XAS spectrum involves an electric-dipole-allowed $2p^63d^0 \rightarrow 2p^53d^1$ transition. To determine the various contributions of the $2p^53d^1$ and $2p^53d^2\underline{L}$ final-state configurations, one needs to project each onto the final-state functions. This is accomplished by a fictitious monopole transition between two noninteracting s orbitals that do not influence the excited $2p^53d^1$ configurations: $2p^53d^1s^2s^0 \rightarrow 2p^53d^1s^1s^1$. When all interactions but the crystal field and the 2p spin−orbit coupling are switched off for the initial state of this fictitious transition, each initial state consists of only one configuration. For Ti(IV), these are $2p_{3/2}3d^1(t_{2g}^1e_g^0)$, $2p_{1/2}3d^1(t_{2g}^1e_g^0)$, $2p_{3/2}3d^1(t_{2g}^0e_g^1)$, $2p_{1/2}3d^1(t_{2g}^0e_g^1)$, $2p_{3/2}3d^2\underline{L}(t_{2g}^2e_g^0)$, $2p_{1/2}3d^2\underline{L}$ $(t_{2g}^2e_g^0)$, $2p_{3/2}3d^2\underline{L}(t_{2g}^1e_g^1)$, $2p_{1/2}3d^2\underline{L}$ $(t_{2g}^1e_g^1)$, $2p_{3/2}3d^2\underline{L}(t_{2g}^0e_g^2)$, and $2p_{1/2}3d^2\underline{L}$ $(t_{2g}^0e_g^2)$. All final states can be projected in terms of these initial configurations and plotted separately. Using this method, the relative weight of all configurations in each final state is determined, and final-state configuration contributions can be generated. Details on the final-state projection method are given in the Supporting Material.

III. RESULTS AND DISCUSSION

1. $3d^0$ without Charge Transfer. The crystal field multiplet Hamiltonian consists of the atomic Hamiltonian plus an electrostatic field. The atomic part contains the Coulomb and exchange interaction (two-electron Slater−Condon integrals) between the single 3d electron and the 2p hole. as well as the spin−orbit couplings of the 2p and 3d electrons. The crystal field part is described by the crystal field parameter 10Dq for cubic symmetry.[2]

When a cubic crystal field is applied to a $3d^0$ system such as $Ti(IV)O_2$, seven final states can be reached.[34] Because the ground state of a $3d^0$ system in a cubic environment has A_{1g} symmetry, and the electric dipole operator has T_{1u} symmetry, all final states that lead to a nonvanishing XAS intensity also have T_{1u} symmetry. Each of these states is a mixture of the various final-state configurations containing either a $3d(t_{2g})$ or $3d(e_g)$ electron (top half of Table S1). Following group theory, there are seven T_{1u}-allowed transitions, four into the t_{2g}, and three in the e_g. However, this does not reflect the corresponding XAS intensity because the electric dipole operator that couples the ground with the excited states is nonisotropic.

As described above, the character of the excited-state wave functions depends on a range of interactions, which influence the spectral shape, and the character of the final-state wave functions will be discussed in a stepwise manner below.

In a first step, the 3d and 2p spin−orbit coupling were excluded, and the strength of the 2p3d Coulomb repulsion varied. Figure 2 (left) shows the calculated absorption spectra for a range of rescaling factors of the 2p Coulomb repulsion (Slater−Condon parameter) to their Hartree−Fock values. Thus, the shape of the spectra is only determined by the constant cubic crystal field 10Dq (set to 2.0 eV) and the strength of the 2p3d Coulomb and exchange interaction. The bottom curve shows the $2p^63d^0 \rightarrow 2p^53d^1$ absorption spectrum with the Slater−Condon parameters rescaled to 0%, i.e., an independent particle description. Thus, two transitions are visible with an intensity ratio of 3/2, which corresponds to the number of empty t_{2g} and e_g orbitals in the ground state. In

DOI: 10.1021/acs.jpcb.5b04133
J. Phys. Chem. B 2015, 119, 13852−13858

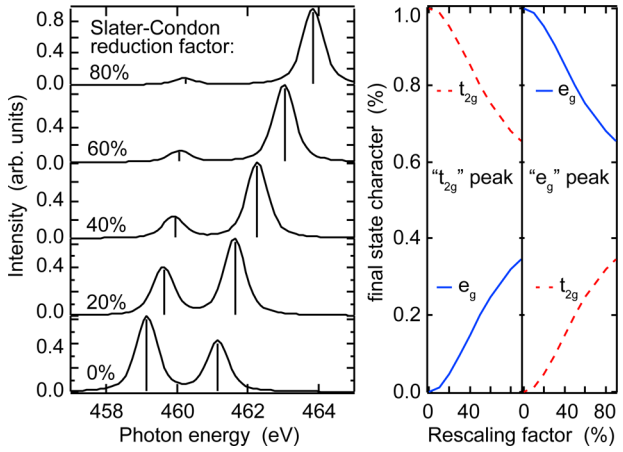

Figure 2. Left: multiplet calculations for the $2p^63d^0 \rightarrow 2p^53d^1$ transition in Ti(IV) without 2p spin−orbit coupling for 0%, 20%, 40%, 60%, and 80% rescaling factors from the Hartree−Fock values for the 3d3d and 2p3d interaction. Right: final-state character for both peaks separated by t_{2g} (red dashed lines) and e_g (blue solid lines) character.

Figure 2 (right), the amount of t_{2g} and e_g character in these two final states is shown, where the orbital character is determined from the final state by analyzing the character of the components. For a rescaling of 0%, the low-energy final state has 100% t_{2g} character, while the high-energy final state consists of 100% e_g character. Note that due to the lack of two-electron matrix elements (the 2p3d Coulomb repulsion), the low-energy peak ("t_{2g}") contains four T_{1u} states, and the high-energy peak ("e_g") contains three T_{1u} states.

With increasing 2p3d Coulomb repulsion, the absorption spectrum still consists of only two peaks with a gradual decrease of their intensity ratio from 3/2 for 0% rescaling to 0.09 for 80% rescaling. When looking at the corresponding final-state characters (Figure 2 (right)), an increase in mixed character is observed, with the initial description still being strongest. This emphasizes the importance of the 2p3d Coulomb repulsion for the character of the final-state wave functions.

While for 0% reduction of the Slater−Condon parameters, the two final states are 4- and 3-fold degenerate, the degeneracy is lifted for any reduction larger than zero (see Figure S1 in the Supporting Information). Only two of these seven states can be reached in an electric-dipole-allowed L-edge XAS excitation. The reason for this lies in the exclusion of 2p spin−orbit coupling. Because the spin of the excited electron is conserved, only a singlet spin coupling can be reached, while the triplet spin coupling is only accessible via 2p spin−orbit coupling.

In the next step, the 2p spin−orbit coupling is included, splitting the 2p levels into $2p_{3/2}$ at lower and $2p_{1/2}$ at higher transition energies. The spin−orbit coupling constant $\lambda = 3.776$ eV is only slightly stronger than the crystal field (2 eV in this case) and comparable to the Slater−Condon parameters for Ti(IV) (values are given in the Supporting Information). It can thus be expected that additional mixing occurs.

In Figure 3 (top), the result for a $2p^63d^0 \rightarrow 2p^53d^1$ absorption including 2p spin−orbit coupling for a range of scaling factors of the Slater−Condon parameters is shown. For 0% scaling, no t_{2g}−e_g mixing occurs, resulting in a t_{2g}/e_g absorption intensity ratio of 3/2 and an L_3/L_2 ratio of 2:1. With increasing scaling of the 2p3d Coulomb repulsion, the t_{2g}/e_g intensity ratio changes in favor of the high-energy "e_g" peaks

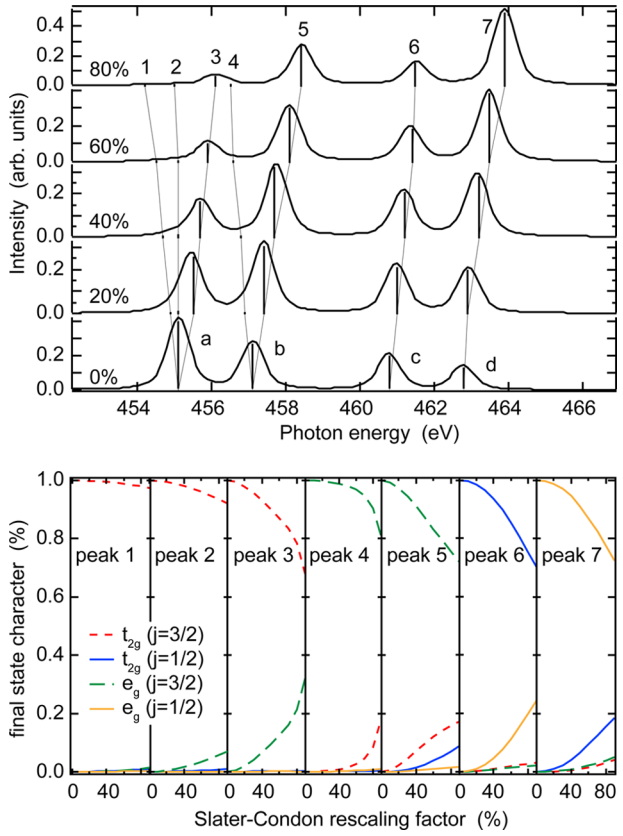

Figure 3. Top: multiplet calculations for the $2p^63d^0 \rightarrow 2p^53d^1$ transition in Ti(IV) for 0%, 20%, 40%, 60%, and 80% rescaling factors from the Hartree−Fock values. Bottom: illustration of the final-state character for all seven peaks as a function of the rescaling factor.

as observed above (Figure 3 (top)). The L_3/L_2 ratio also changes from 2:1 down to 0.54:1 for an 80% scaling, which is in line with previous results.[34] In addition, all seven final states are reached via the electric dipole transition due to the inclusion of the 2p spin−orbit coupling and the transition to jj coupling. This is illustrated in Figure 3 (top) by the thin gray lines. The low-energy t_{2g} peak (a) splits into three lines, while the low-energy e_g peak (b) splits into two lines according to group theory. The high-energy t_{2g} (c) and e_g (d) peaks each consists of only one final state and thus do not split.

The character distribution of the four final-state configurations in each of the seven lines is given in Figure 3 (bottom). For 0% scaling, only four lines are visible with 100% character of the expected configurations: $2p_{3/2}^{5}3d^1(t_{2g}^{1})$, $2p_{3/2}^{5}3d^1(e_g^{1})$, $2p_{1/2}^{5}3d^1(t_{2g}^{1})$, and $2p_{1/2}^{5}3d^1(e_g^{1})$, where the first low-energy line is 3-fold degenerate and the second line is 2-fold degenerate. When the scaling of the Slater−Condon parameters is increased, the different final-state characters get mixed due to the two-electron Coulomb repulsion matrix elements.

As seen in Figure 3 (bottom), for the seven final states, the nominal character is strongest for all scaling factors, but significant mixing is visible. While final states 1 and 2 consist almost exclusively of $2p_{3/2}^{5}3d^1(t_{2g}^{1})$, peak 3 also contains a strong amount of $2p_{3/2}^{5}3d^1(e_g^{1})$ character. Final states 4 and 5 have predominantly $2p_{3/2}^{5}3d^1(e_g^{1})$ character, both with a significant amount of $2p_{3/2}^{5}3d^1(t_{2g}^{1})$. However, final state 5 also contains $2p_{1/2}^{5}$ character, especially $2p_{1/2}^{5}3d^1(t_{2g}^{1})$. Final states 6 and 7 both contain a small amount of $j = 3/2$ character.

DOI: 10.1021/acs.jpcb.5b04133
J. Phys. Chem. B 2015, 119, 13852−13858

With the crystal field being of the same order as the 2p spin−orbit coupling, variations in both lead to variations in the spectral shape as well as the final-state character distribution of the seven final states. These are shown in Figure S2. An increase in the 2p spin−orbit coupling strength leads to an increased energy splitting of the L_3 and L_2 edge together with an increase of the L_3/L_2 intensity ratio in agreement with the previous results.[34] Note that the presented calculations are valid for d^0 systems, making an increase in the spin−orbit coupling strength applicable to systems such as V^{5+} or Zr^{4+} but not for open-shell systems.

As noted above, the intensity-weighted final-state character distribution does not conserve the expected t_{2g}/e_g character ratio of 3/2 as seen in the independent particle solution. The crystal field and 2p3d Coulomb repulsion are of the same order of magnitude. While the crystal field separates t_{2g} and e_g character, they mix in the final states through the 2p3d interactions, and intensity transfer between states within the same symmetry can occur. The fact that the mixing of t_{2g} and e_g character in the final states does not conserve the 3/2 ratio likely reflects the nature of the 2p orbitals, which contribute to the strength of the dipole transition matrix elements.[7] Note that this is not the case for a 1s core-hole, for which the 1s3d interaction is very weak. Therefore, the 3/2 final-state character ratio is preserved in metal K-pre-edges.[35]

2. $3d^0$ including Charge Transfer. When ligand-to-metal charge-transfer effects are included, a two-configuration model is used to describe the ground and excited states in the L-edge XAS process: $\alpha(3d^0 + \beta\, 3d^1\underline{L}) \rightarrow \gamma(2p^5 3d^1) + \delta(2p^5 3d^2\underline{L})$. The ground-state wave function is then a linear combination of the three possible configurations $3d^0$, $3d^1\underline{L}(t_{2g}^1)$, and $3d^1\underline{L}(e_g^1)$, while the L-edge absorption final states are linear combinations of the final-state configurations $2p^5 3d^1(t_{2g}^1)$, $2p^5 3d^1(e_g^1)$, $2p^5 3d^2\underline{L}(t_{2g}^2)$, $2p^5 3d^2\underline{L}(t_{2g}^1 e_g^1)$, and $2p^5 3d^1\underline{L}(e_g^2)$. Because the 2p spin−orbit coupling splits the 2p into $2p_{3/2}$ and $2p_{1/2}$ in jj coupling, 10 final-state configurations are present.

Besides the assignment of features in the absorption spectrum to their final-state metal characters as described above, knowledge of their character in terms of the ligand configuration is equally important. A series of L-edge absorption spectra calculated for three values of the charge-transfer energy Δ together with the corresponding final-state characters is shown in Figure 4. A single value of Δ for both the e_g and t_{2g} sub-bands has been employed. For oxide complexes, essentially all L-edge multiplet calculations are performed with one charge-transfer state that represents the oxygen 2p band; hence, only one charge-transfer energy Δ is used in this study. It is assumed that the oxygen 2p valence band states that mix with the transition metal e_g states are equivalent in energy with those that mix with the metal t_{2g} states, and variations are taken into account by varying the initially chosen 2:1 ratio of the e_g and t_{2g} mixing parameters. Note that in RIXS experiments on oxides such as NiO, one observes two charge-transfer peaks that can be related to different ligand (sub)-bands, which have been simulated by taking the band structure of the sp electrons as a large number of different charge-transfer states.[36] In molecular systems, the difference in energy between t_{2g} and e_g ligand orbitals is often accounted for by either applying two different charge-transfer energies Δ or varying the corresponding mixing parameter,[6] resulting in a strong deviation of the initially chosen 2:1 ratio of the e_g and t_{2g} mixing parameters.

The values of Δ chosen in Figure 4 were −2, 2, and 6 eV and represent the difference between the center-of-mass of the two configurations d^0 and $d^1\underline{L}$. Values of the effective charge-transfer energy Δ_{eff}, which is the difference between the lowest energies of the two sets of multiplets, were −2.65, 1.35, and 5.35 eV. The crystal field value 10Dq was set to 2.0 eV, and the e_g and t_{2g} mixing parameters $T(e_g)$ and $T(t_{2g})$ were set to 2.0 and 1.0 eV, respectively. The Slater−Condon parameters were rescaled to 80% of their Hartree−Fock values. The resulting spectra show only small variations in shape and intensity throughout the series; mainly, peaks get sharper with increasing charge-transfer energy Δ, i.e., with increasing ionic character, which is in line with the solid-state effects described above.[34] Note that all spectra have been shifted such that their most intense peak aligns at 463.8 eV.

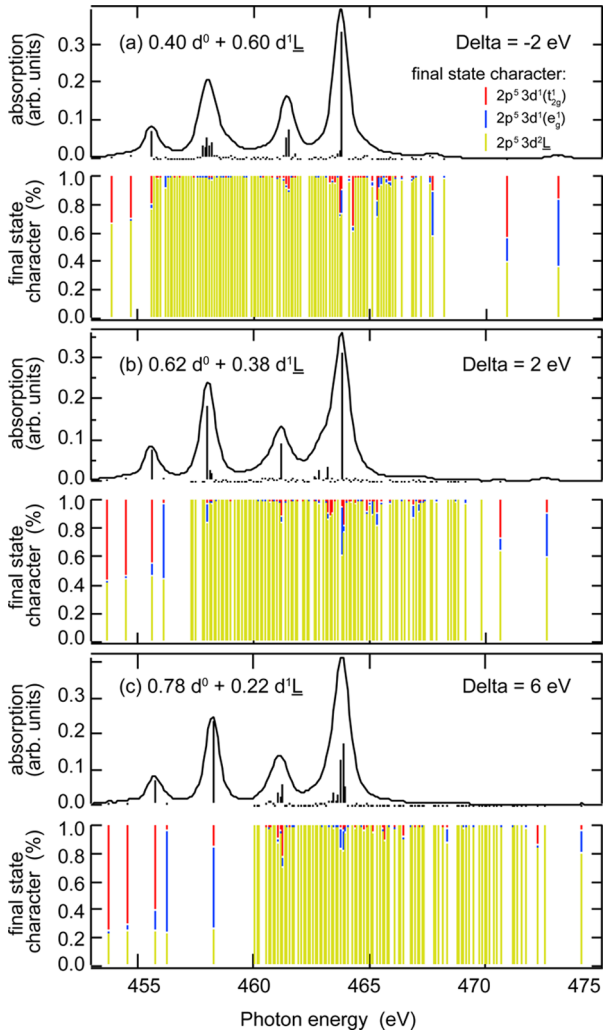

Figure 4. Simulated spectra for Δ = −2 (top), 2 (middle), and 6 eV (bottom). The vertical lines in the absorption spectra represent the L-edge XAS intensity. The percentage of the final-state character distribution of each line is given below the corresponding spectrum, separated into three configurations: $2p^5\ 3d^1(t_{2g})$ (red), $2p^5\ 3d^1(e_g)$ (blue), and $2p^5\ 3d^2\underline{L}$ (light green).

The effect of Δ is prominent in the ground-state configuration weights. For Δ = −2 eV, the ground-state wave function is more ligand in character, with only 40% d^0 and 60% $d^1\underline{L}$ (32% t_{2g}, 28% e_g) configuration weight. For Δ = 2 eV, this inverts to 62% d^0 and 38% $d^1\underline{L}$ (16% t_{2g}, 22% e_g). A large amount of ligand character of 22% $d^1\underline{L}$ (8% t_{2g}, 14% e_g) is still present in the ground-state wave function for Δ = 6 eV.

DOI: 10.1021/acs.jpcb.5b04133
J. Phys. Chem. B 2015, 119, 13852−13858

As described above, for the $2p^5 3d^1$ t_{2g} and e_g transitions, the ratio of T_{1u} final states is 4:3. This ratio has to be expanded to include the charge-transfer final states $2p^5$ $3d^2\underline{L}$, giving a ratio of 4:3:337 for ($2p^5 3d^1(t_{2g})$:$2p^5 3d^1(e_g)$:$2p^5 3d^2\underline{L}$). A full separation of this ratio, taking into account the 2p spin−orbit coupling as well as the various charge-transfer final-state configurations, is given in Table S1.

The vertical lines shown in Figure 4 represent either the absorption intensity that is reached in the electric-dipole-allowed transition (top part in each subfigure) or the amount of configuration character in each final state (bottom part of each subfigure). The sum of all characters for each final state thus sums to 1. In Figure 4, the final-state characters are projected into the three configuration weights of $2p^5 3d^1(t_{2g})$, $2p^5 3d^1(e_g)$, and $2p^5 3d^2\underline{L}$.

It is observed that states with predominantly ligand character shift toward high energies with increasing values of Δ. While at Δ = −2 eV the low-energy states show their expected metal character, which increases with increasing Δ, the higher states are dominated by ligand character. This is expected for all additional lines as compared to the noncharge-transfer calculations above (Figure 1 and 3). For the intense lines in the "t_{2g}" and the "e_g" peak regions, however, this leads to interesting effects. These are most prominent around the formal L_2 "e_g" peak at 463.8 eV, where even at Δ = 6 eV its final-state character is dominated by ligand contributions. This reflects the mixing of shake-up states into the main lines at higher energies, leading to their increased ligand character despite a high value of Δ.

For closer insight, Figure 5 focuses on the L_2 edge between 458 and 466 eV for the same values of Δ as above. The intense lines (plotted in red) are separately analyzed, and the relative weight of each of the 10 configurations in the corresponding final state is plotted below.

For Δ = −2 eV (Figure 5, top), the peak at 461.4 eV (L_2 "t_{2g}" in Figure 1) consists of two lines with a similar final-state character pattern. In both, the strongest configuration is the $2p^5_{3/2}3d^2\underline{L}(e_g^2)$ shake-up from the L_3 edge (52% and 39%), followed by the $2p^5_{3/2}3d^2\underline{L}(t_{2g}^1e_g^2)$ shake-up (14% and 20%) and the $2p^5_{1/2}3d^2\underline{L}(t_{2g}^2)$ charge-transfer part (13% and 15%). For Δ = 2 eV (Figure 5, middle), the $2p^5_{3/2}3d^2\underline{L}(t_{2g}^1e_g^1)$ shake-up dominates this final state (45%), followed by the $2p^5_{1/2}3d^1(t_{2g}^1)$ main line (17%). When Δ is further increased to 6 eV (Figure 5, bottom), the main line $2p^5_{1/2}3d^1(t_{2g}^1)$ configuration weight decreases (10% and 22%) due to the large amount of the $2p^5_{3/2}3d^2\underline{L}(t_{2g}^2)$ shake-up (75% and 54%). While the final state of the peak previously described as L_2 "t_{2g}" indeed mostly contains $2p^5_{1/2}3d^1(t_{2g}^1)$ character without including charge transfer, this changes dramatically when ligand mixing is included. Now this peak is dominated by the shake-ups $2p^5_{3/2}3d^2\underline{L}(e_g^2)$, $2p^5_{3/2}3d^2\underline{L}(t_{2g}^1e_g^1)$, and $2p^5_{3/2}3d^2\underline{L}(t_{2g}^2)$ depending on the value of Δ.

For the higher-energy peak at 463.8 eV (L_2 "e_g" in Figure 1) a different character pattern of the corresponding final states is observed. For Δ = −2 eV (Figure 5, top) this peak mostly contains one final state, with mostly $2p^5_{3/2}3d^2\underline{L}(t_{2g}^1e_g^1)$ shake-up (45%), followed by the $2p^5_{1/2}3d^1(e_g^1)$ main line (16%). For Δ = 2 eV (Figure 5, middle), this ratio inverts, with the $2p^5_{1/2}3d^1(e_g^1)$ main line being the highest final-state configuration weight (32%), followed by the $2p^5_{3/2}3d^2\underline{L}(t_{2g}^1e_g^1)$ shake-up (20%). In addition, this state also contains some $2p^5_{3/2}3d^2\underline{L}(e_g^2)$ shake-up character (15%). For Δ = 6 eV, the peak at 463.8 eV mainly consists of two final states, in which the amount of the $2p^5_{1/2}3d^1\underline{L}(e_g^1)$ main line character decreases again (13% and 15%), as these final states are dominated by the $2p^5_{3/2}3d^2\underline{L}$-$^1_{2g}e_g^1$) shake-up character (69% and 62%). Thus, the character of the final states in the L_2 "e_g" peak differs significantly from that of the L_2 "t_{2g}" peak. While the latter consists mostly of shake-up lines, the L_2 "e_g" peak final-state character varies depending on the value of the charge-transfer energy.

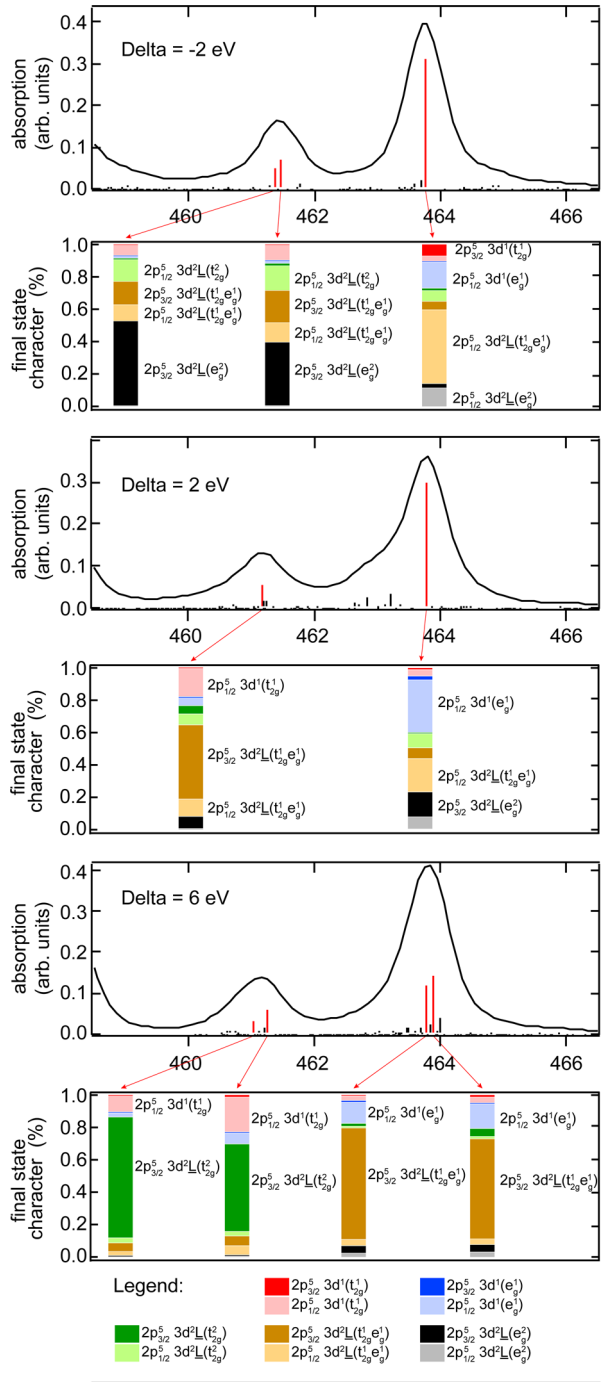

Figure 5. Enlarged image of the L_2-edge region of the L-edge XAS spectrum for Δ = −2 (top), 2 (middle), and 6 eV (bottom). The vertical lines in the absorption spectra represent the L-edge XAS intensity. The distribution of the final-state characters for selected final states (indicated as red vertical lines) are given below the corresponding absorption spectrum.

DOI: 10.1021/acs.jpcb.5b04133
J. Phys. Chem. B 2015, 119, 13852−13858

Also, the two main peaks in the L_3-edge region show a variation of final-state character depending on the charge-transfer energy, which is shown in a similar way as Figure 5 in Figure S3. The amount of $2p^5_{3/2}3d^1(t^1_{2g})$ final-state character in the L_3 "t_{2g}" monotonically increases for the three selected Δ values: −2, 2, and 6 eV. In contrast, the L_3 "e_g" peak is dominated by charge-transfer character throughout the series. For Δ = −2 eV, the two main final-state characters are $2p^5_{3/2}3d^2\underline{L}(t^2_{2g})$ and $2p^5_{3/2}3d^2\underline{L}(t^1_{2g}e^1_g)$. For Δ = 2 eV, the $2p^5_{3/2}3d^2\underline{L}(t^1_{2g}e^1_g)$ configuration character dominates the two main final states; this changes mostly to $2p^5_{3/2}3d^2\underline{L}(e^2_g)$ for Δ = 6 eV.

From ab initio calculations, final-state configuration weights for 2p L-edge calculations of Ti d^0 including charge-transfer interactions have been determined.[17,18,20,24] Similar to the results presented here, $3d^1$ final-state configuration intensities are found predominantly around the expected energies, with low-intensity contributions in other energy regions. The charge-transfer $3d^2\underline{L}$ final-state configuration weights are distributed over a larger energy range as well as at higher energies.

For energies higher than the L_2 "e_g" peak energy at 463.8 eV, additional intensity is found (see Figure 3; an expanded version is shown in the Figure S4). These higher-energy lines with some intensity have previously been identified as polaronic satellites[37] originating from the polarization of the ligand oxygen ions by the metal core-hole. In the present study, these satellites are obtained from the charge-transfer mixing, emphasizing the ligand covalency as the origin of these features. Their shape and configuration spectral weight depend on the value of Δ, with final-state configuration character reflecting a high amount of ligand mixing.

Similar to the noncharge-transfer case above, variations in the strength of the 2p spin−orbit coupling, the ligand crystal field 10Dq, and the reduction of the Slater−Condon parameters strongly influence the spectral shape and final-state configuration character. While the general effects of 2p spin−orbit coupling and the crystal field strength variations are similar to the noncharge-transfer case (see Figure S2), a reduction of the Slater−Condon parameter is often coupled to the degree of covalency. Figure S5 shows a collection of L-edge curves for a range of Slater−Condon reduction values for Δ = 2.0 eV. A similar trend as in Figure 3 is observed. In the physically interesting region of around 80% reduction factor, the variations in the spectral shape when charge transfer is included are small, emphasizing the correlation of charge transfer and the screening of Coulomb repulsion.

Following the sum rule, the full intensity, i.e., the area under the spectral curve, when properly normalized, is proportional to the effective number of holes.[6,38,39] Thus, the integration over all final states relates to the metal d-character averaged over all orbitals in the ground state and can be determined directly from the experimental result. Because the ground state is not affected by the strong 2p3d interaction, an analysis in terms of ground-state differential orbital covalency[6] is achieved through fitting the experimental L-edge XAS by charge-transfer multiplet calculations without specific final-states assignment. The spectral shape, however, is given by the final states, for which the configuration characters are investigated in this study. The final-state characters, which determine the spectral features, exhibit a complex behavior that does not allow a direct interpretation of experimental L-edge absorption spectra in terms of final-state configuration weight without the above projection analysis.

IV. SUMMARY

The final-state projection method implemented in the TT-multiplet code allows for a configuration analysis for each L-edge XAS final state. The method has been used to separate each possible final-state configuration in the 2p absorption spectrum for Ti(IV) (d^0) in an O_h ligand field without and with charge-transfer effects. The importance of the 2p3d Coulomb repulsion and 2p spin−orbit coupling on the spectral shape and mixing of configuration weight among final states has been demonstrated.

The ligand-hole $3d^2\underline{L}$ configuration weight in each final state has been found to show a complex behavior with strong contributions of the shake-up states in the higher-energy final states, especially in the L_2-edge region. This leads to a significant redistribution of final-state characters even for included charge-transfer mixing.

■ ASSOCIATED CONTENT

Supporting Information

The Supporting Information is available free of charge on the ACS Publications website at DOI: 10.1021/acs.jpcb.5b04133.

Details on the theoretical method are given, together with a collection of necessary input files (.rcg, .rac, and .ban). Additional figures are given for the cases of (i) excluding charge transfer for varying the reduction of the Slater−Condon parameters, the strength of the 2p spin−orbit coupling, and ligand crystal field; and (ii) including charge transfer for a blow-up of the final-state configuration character distribution in the L_2-edge satellite region, and for a series of varying reduction factors of the Slater−Condon parameters. (PDF)

■ AUTHOR INFORMATION

Corresponding Authors

*tkroll@slac.stanford.edu
*f.m.f.degroot@uu.nl
*edward.solomon@stanford.edu.

Notes

The authors declare no competing financial interest.

■ ACKNOWLEDGMENTS

Financial support from the German Research Foundation (D.F.G.) under grant number KR3611/2-1 and from the Human Frontier Science Program grant RCP0063/2013 (T.K.) is greatly acknowledged. This research was supported by the National Institute of General Medical Sciences of the National Institutes of Health under award number R01GM040392 (E.I.S.). It was mainly performed at the Linac Coherent Light Source (LCLS), Directorate of SLAC National Accelerator Laboratory and Office of Science User Facility, which is operated by Stanford University for the U.S. Department of Energy (DOE) Office of Science, Office of Basic Energy Science under contract number DE-AC02-76SF00515.

■ REFERENCES

(1) de Groot, F. M. F.; Figueiredo, M. O.; Basto, M. J.; Abbate, M.; Petersen, H.; Fuggle, J. C. 2*p* X-ray absorption of titanium in minerals. *Phys. Chem. Miner.* **1992**, *19*, 140−147.

DOI: 10.1021/acs.jpcb.5b04133
J. Phys. Chem. B 2015, 119, 13852−13858

(2) de Groot, F. M. F.; Kotani, A. *Core Level Spectroscopy of Solids*; CRC Press: Boca Raton, FL, 2008.
(3) van der Laan, G.; Thole, B. J. Local Probe for Spin-Orbit Interaction. *Phys. Rev. Lett.* **1988**, *60*, 1977.
(4) Thole, B. T.; van der Laan, G.; Butler, P. H. Spin-mixed ground state of Fe phthalocyanine and the temperature-dependent branching ratio in X-ray absorption spectroscopy. *Chem. Phys. Lett.* **1988**, *149*, 295−299.
(5) Wang, H.; Patil, D. S.; Gu, W.; Jacquamet, L.; Friedrich, S.; Funk, T.; Cramer, S. P. L-edge X-ray absorption spectroscopy of some Ni enzymes: Probe of Ni electronic structure. *J. Electron Spectrosc. Relat. Phenom.* **2001**, *114*, 855−863.
(6) Wasinger, E. C.; de Groot, F. M. F.; Hedman, B.; Hodgson, K. O.; Solomon, E. I. L-edge X-ray Absorption Spectroscopy of Non-Heme Iron Sites: Experimental Determination of Differential Orbital Covalency. *J. Am. Chem. Soc.* **2003**, *125*, 12894−12906.
(7) Kroll, T.; Kraus, R.; Schöenfelder, R.; Aristov, V. Yu.; Molodtsova, O. V.; Hoffmann, P.; Knupfer, M. Transition metal phthalocyanines: Insight into the electronic structure from soft x-ray spectroscopy. *J. Chem. Phys.* **2012**, *137*, 054306.
(8) Wilson, S. A.; Kroll, T.; Decreau, R. A.; Hocking, R. K.; Lundberg, M.; Hedman, B.; Hodgson, K. O.; Solomon, E. I. Iron L-Edge X-ray Absorption Spectroscopy of Oxy-Picket Fence Porphyrin: Experimental Insight into Fe−O_2 Bonding. *J. Am. Chem. Soc.* **2013**, *135*, 1124−1136.
(9) de Groot, F. M. F.; Fuggle, J. C.; Thole, B. T.; Sawatzky, G. A. 2*p* x-ray absorption of 3*d* transition-metal compounds: An atomic multiplet description including the crystal field. *Phys. Rev. B: Condens. Matter Mater. Phys.* **1990**, *42*, 5459.
(10) Arrio, M.-A.; Sainctavit, Ph.; Cartier dit Moulin, Ch.; Mallah, T.; Verdaguer, M.; Pellegrin, E.; Chen, C. T. Characterization of Chemical Bonds in Bimetallic Cyanides Using X-ray Absorption Spectroscopy at $L_{2,3}$ Edges. *J. Am. Chem. Soc.* **1996**, *118*, 6422−6427.
(11) Haverkort, M. W.; Hu, Z.; Cezar, J. C.; Burnus, T.; Hartmann, H.; Reuther, M.; Zobel, C.; Lorenz, T.; Tanaka, A.; Brookes, N. B.; et al. Spin State Transition in LaCoO3 Studied Using Soft X-ray Absorption Spectroscopy and Magnetic Circular Dichroism. *Phys. Rev. Lett.* **2006**, *97*, 176405.
(12) van der Laan, G.; Kirkman, I. W. The 2p absorption spectra of 3d transition metal compounds in tetrahedral and octahedral symmetry. *J. Phys.: Condens. Matter* **1992**, *4*, 4189.
(13) Kroll, T.; Aristov, V. Yu.; Molodtsova, O. V.; Ossipyan, Yu. A.; Vyalikh, D. V.; Büchner, B.; Knupfer, M. Spin and Orbital Ground State of Co in Cobalt Phthalocyanine. *J. Phys. Chem. A* **2009**, *113*, 8917−8922.
(14) Stepanow, S.; Miedema, P. S.; Mugarza, A.; Ceballos, G.; Moras, P.; Cezar, J. C.; Carbone, C.; de Groot, F. M. F.; Gambardella, P. Mixed-valence behavior and strong correlation effects of metal phthalocyanines adsorbed on metals. *Phys. Rev. B: Condens. Matter Mater. Phys.* **2011**, *83*, 22040(R).
(15) Ikeno, H.; Tanaka, I.; Koyama, Y.; Mizoguchi, T.; Ogasawara, K. First-principles multielectron calculations of Ni $L_{2,3}$ NEXAFS and ELNES for $LiNiO_2$ and related compounds. *Phys. Rev. B: Condens. Matter Mater. Phys.* **2005**, *72*, 075123.
(16) Ikeno, H.; Mizoguchi, T.; Koyama, Y.; Kumagai, Y.; Tanaka, I. First-principles multi-electron calculations for $L_{2,3}$ ELNES/XANES of 3d transition metal monoxides. *Ultramicroscopy* **2006**, *106*, 970−975.
(17) Ikeno, H.; de Groot, F. M. F.; Stavitski, E.; Tanaka, I. Multiplet calculations of $L_{2,3}$ x-ray absorption near-edge structures for 3d transition-metal compounds. *J. Phys.: Condens. Matter* **2009**, *21*, 104208.
(18) Laskowski, R.; Blaha, P. Understanding the L2,3 x-ray absorption spectra of early 3dtransition elements. *Phys. Rev. B: Condens. Matter Mater. Phys.* **2010**, *82*, 205104.
(19) De Francesco, R.; Stener, M.; Fronzoni, G. Computational investigation of the $L_{2,3}$-edge spectra of bulk and (110) surface of rutile TiO_2. *Surf. Sci.* **2011**, *605*, 500−506.
(20) Ikeno, H.; Mizoguchi, T.; Tanaka, I. Ab initio charge transfer multiplet calculations on the L2,3 XANES and ELNES of 3d transition metal oxides. *Phys. Rev. B: Condens. Matter Mater. Phys.* **2011**, *83*, 155107.
(21) Landmann, M.; Rauls, E.; Schmidt, W. G. J. The electronic structure and optical response of rutile, anatase and brookite TiO_2. *J. Phys.: Condens. Matter* **2012**, *24*, 195503.
(22) Haverkort, M. W.; Zwierzycki, M.; Andersen, O. K. Multiplet ligand-field theory using Wannier orbitals. *Phys. Rev. B: Condens. Matter Mater. Phys.* **2012**, *85*, 165113.
(23) Roemelt, M.; Maganas, D.; DeBeer, S.; Neese, F. A combined DFT and restricted open-shell configuration interaction method including spin-orbit coupling: Application to transition metal L-edge X-ray absorption spectroscopy. *J. Chem. Phys.* **2013**, *138*, 204101.
(24) Maganas, D.; DeBeer, S.; Neese, F. Restricted Open-Shell Configuration Interaction Cluster Calculations of the L-Edge X-ray Absorption Study of TiO_2 and CaF_2 Solids. *Inorg. Chem.* **2014**, *53*, 6374−6385.
(25) Pinjari, R. V.; Delcey, M. G.; Guo, M.; Odelius, M.; Lundberg, M. Restricted active space calculations of L-edge x-ray absorption spectra: From molecular orbits to multiplet states. *J. Chem. Phys.* **2014**, *141*, 124116.
(26) Stavitski, E.; de Groot, F. M. F. The CTM4XAS program for EELS and XAS spectral shape analysis of transition metal L-edges. *Micron* **2010**, *41*, 687−694.
(27) Cowan, R. D. *The Theory of Atomic Structure and Spectra*; University of California Press: Berkeley, CA, 1981.
(28) Butler, P. H. Point Group Symmetry: Applications. In *Methods and Tables*; Plenum Press: New York, 1981.
(29) van der Laan, G.; Kirkman, I. W. The 2p absorption spectra of 3d transition metal compounds in tetrahedral and octahedral symmetry. *J. Phys.: Condens. Matter* **1992**, *4*, 4189.
(30) Arrio, M.-A.; Scuiller, A.; Sainctavit, P.; Cartier dit Moulin, C.; Mallah, T.; Verdaguer, M. Soft X-ray Magnetic Circular Dichroism in Paramagnetic Systems: Element-Specific Magnetization of Two Heptanuclear Cr^{III} M^{II}_6 High-Spin Molecules. *J. Am. Chem. Soc.* **1999**, *121*, 6414−6420.
(31) Cartier dit Moulin, C.; Villain, F.; Bleuzen, A.; Arrio, M.-A.; Sainctavit, P.; Lomenech, C.; Escax, V.; Baudelet, F.; Dartyge, E.; Gallet, J.-J.; et al. Photoinduced Ferrimagnetic Systems in Prussian Blue Analogues $C^I_xCo_4[Fe(CN)_6]_y$ (C^I = Alkali Cation). 2. X-ray Absorption Spectroscopy of the Metastable State. *J. Am. Chem. Soc.* **2000**, *122*, 6653−6658.
(32) Thole, B. T.; van der Laan, G.; Fuggle, J. C.; Sawatzky, G. A.; Karnatak, R. C.; Esteva, J.-M. 3d x-ray-absorption lines and the $3d^94f^{n+1}$ multiplets of the lanthanides. *Phys. Rev. B: Condens. Matter Mater. Phys.* **1985**, *32*, 5107.
(33) Green, R. J.; Zatsepin, D. A.; St. Onge, D. J.; Kurmaev, E. Z.; Gavrilov, N. V.; Zatsepin, A. F.; Moewes, A. Electronic band gap reduction and intense luminescence in Co and Mn ion-implanted SiO_2. *J. Appl. Phys.* **2014**, *115*, 103708.
(34) Zaanen, J.; Sawatzky, G. A.; Fink, J.; Speier, W.; Fuggle, J. C. $L_{2,3}$ absorption spectra of the lighter *3d* transition metals. *Phys. Rev. B: Condens. Matter Mater. Phys.* **1985**, *32*, 4905.
(35) Westre, T.; Kennepohl, P.; DeWitt, J. G.; Hedman, B.; Hodgson, K. O.; Solomon, E. I. A Multiplet Analysis of Fe K-Edge 1s → 3d Pre-Edge Features of Iron Complexes. *J. Am. Chem. Soc.* **1997**, *119*, 6297−6314.
(36) Green R. Transition Metal Impurities in Semiconductors: Induced Magnetism and Band Gap Engineering. *PhD Thesis*, University of Saskatchewan, 2013.
(37) van der Laan, G. Polaronic satellites in x-ray-absorption spectra. *Phys. Rev. B: Condens. Matter Mater. Phys.* **1990**, *41*, 12366(R).
(38) de Groot, F. M. F.; Grioni, M.; Fuggle, M. C.; Ghijsen, J.; Sawatzky, G. A.; Petersen, H. Oxygen 1s x-ray-absorption edges of transition-metal oxides. *Phys. Rev. B: Condens. Matter Mater. Phys.* **1989**, *40*, 5715.
(39) Kurian, R.; Kunnus, K.; Wernet, P.; Butorin, S. M.; Glatzel, P.; de Groot, F. M. F. Intrinsic deviations in fluorescence yield detected x-ray absorption spectroscopy: the case of the transition metal $L_{2,3}$ edges. *J. Phys.: Condens. Matter* **2012**, *24*, 452201.

DOI: 10.1021/acs.jpcb.5b04133
J. Phys. Chem. B 2015, 119, 13852−13858